Accurate seeing measurements with MASS and DIMM

A. Tokovinin[1]⋆, V. Kornilov[2]†
[1] *Cerro Tololo Inter-American Observatory, Casilla 603, La Serena, Chile*
[2] *Sternberg Astronomical Institute, Universitetsky prosp. 13, 119992 Moscow, Russia*

-

ABSTRACT

Astronomical seeing is quantified by a single parameter, turbulence integral, in the framework of the Kolmogorov turbulence model. This parameter can be routinely measured by a Differential Image Motion Monitor, DIMM. A new instrument, Multi-Aperture Scintillation Sensor (MASS), permits to measure the seeing in the free atmosphere above ∼0.5km and, together with a DIMM, to estimate the ground-layer seeing. The absolute accuracy of both methods is studied here using analytical theory, numerical simulation, and experiments. A modification of the MASS data processing to compensate for partially saturated scintillation is developed. We find that the DIMM can be severely biased by optical aberrations (e.g. defocus) and propagation. Seeing measurements with DIMM and MASS can reach absolute accuracy of ∼10% when their biases are carefully controlled. Pushing this limit to 1% appears unrealistic because the seeing itself is just a model-dependent parameter of a non-stationary random process.

Key words: site testing – atmospheric effects

1 INTRODUCTION

Measurements of astronomical "seeing" are performed for selecting new sites and supporting operation of existing telescopes. Recently, a standard Differential Image Motion Monitor (DIMM) method (Martin 1987; Sarazin & Roddier 1990) has been complemented with a new technique, Multi-Aperture Scintillation Sensor (MASS) (Kornilov et al. 2003). This new instrument is based on the analysis of scintillation and permits to measure the seeing in the free atmosphere, isoplanatic angle, and adaptive-optics (AO) time constant. Both MASS and DIMM require only a small telescope and can be combined in a single instrument (Kornilov et al. 2007). MASS-DIMM site monitors gradually become a new standard.

We can evaluate the ground-layer (GL) seeing produced in the first 0.5 km above the observatory by subtracting the turbulence integrals measured with DIMM and MASS. It is important to measure the GL seeing for evaluating the performance of Ground-Layer Adaptive Optics (GLAO). However, subtraction only works when both methods are accurate, i.e. deliver results on the absolute scale. Absolute accuracy of seeing measurements becomes critical for the site comparison, where the differences are often below 10%.

In principle, both DIMM and MASS should give accurate results when their instrument parameters are set correctly and their intrinsic biases are understood and removed. Here we investigate these biases in detail, quantify them, and propose corrections. Biases of the DIMM method have been already addressed in the literature (Martin 1987; Tokovinin 2002a). We continue by considering additional effects such as light propagation and optical aberrations. The analysis of the MASS method given by Tokovinin et al. (2003) is extended by studying small departures from the weak-scintillation theory which cause a systematic bias, "over-shoots", and can be corrected by a modified data processing.

This work has been stimulated by the need to get accurate results from the existing suite of MASS-DIMM instruments, described in the accompanying paper (Kornilov et al. 2007). Correct setting and operation of these instruments, also critical for getting accurate data, is addressed in that paper. Here we concentrate on the theoretical analysis and simulations, trying to formulate practical recommendations and recipes while avoiding mathematical complexity as much as possible.

We begin by asking the question "what is seeing and how accurately can it be defined and measured?" in Sect. 2. In Sect. 3,

⋆ E-mail: atokovinin@ctio.noao.edu
† E-mail: victor@sai.msu.ru

Table 1. Quantities relevant to seeing

Quantity	Units	Formula
Seeing (FWHM)	rad	$\varepsilon_0 = 0.98\lambda/r_0$
Turbulence integral	m$^{1/3}$	$J = \int_{\text{path}} C_n^2(z)\,dz$
Fried parameter	m	$r_0 = [0.423(2\pi/\lambda)^2 J]^{-3/5}$
		$r_0 = 1.01\lambda/\varepsilon_0$
Phase power spectrum	m^2	$\Phi_\varphi(\boldsymbol{f}) = C\,\|\boldsymbol{f}\|^{-11/3},$
		$C = 0.00969(2\pi/\lambda)^2 J$
		$C = 0.0229 r_0^{-5/3}$

the MASS method is studied under conditions of realistic (not weak) scintillation. Then in Sect. 4 we address two previously neglected effects in a DIMM – propagation and optical aberrations – and show that they can cause a significant bias, in addition to the known DIMM biases. Our conclusions and recommendations are formulated in Sect. 5.

2   WHAT IS MEASURED BY A SEEING MONITOR?

2.1   Turbulence parameters

Turbulence measurements are based on the standard theory (Tatarskii 1961; Roddier 1981). For convenience, major atmospheric parameters are recalled in Table 1. These definitions assume a scale-free Kolmogorov turbulence spectrum with only one parameter, turbulence strength. This single parameter can be expressed equivalently by ε_0, r_0, or J. These quantities (except J) depend on the imaging wavelength λ which is assumed here to be 500 nm if not specified. Accurate measurement of this single parameter (called "seeing" in a broad sense) is the purpose of a seeing monitor. The atmosphere can be split into an arbitrary number of zones (or layers), and we also want to measure the seeing produced by each of the layers – the turbulence profile. Other atmospheric parameters (time constant, isoplanatic angle), not considered here, are also of interest to modern astronomy.

The seeing ε_0 is often considered to be the angular image spread caused by the atmosphere. This interpretation is only approximate because even in a perfect telescope the actual long-exposure point spread function (PSF) depends on several additional parameters (outer scale, wavelength, telescope diameter, guiding). Current seeing monitors measure only one number ε_0 which is necessary, but not sufficient for accurate prediction of the atmospheric PSF or other turbulence-related optical quantities.

It is always implicitly assumed that the statistical properties of turbulence are stationary, while in fact they are not. Any measurement refers only to the particular moment in time and to the particular viewing direction. The non-stationarity precludes very precise measurements of atmospheric parameters because averaging over a larger spatial or temporal sample of turbulence does not lead to the improved statistical precision. This aspect, often overlooked, also makes seeing measurements intrinsically irreproducible. Comparisons between seeing monitors or between
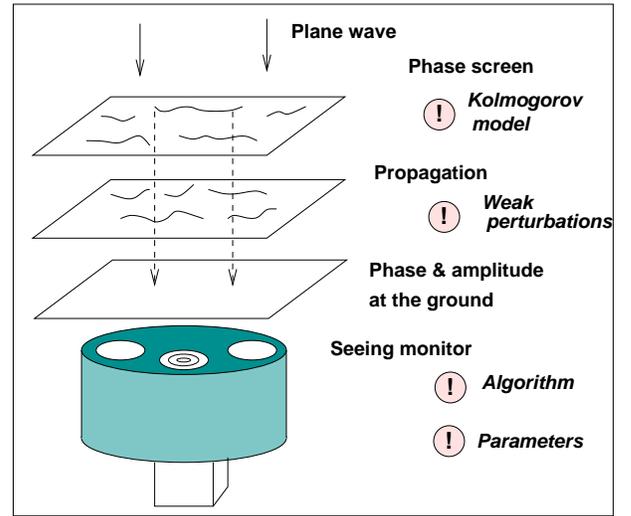

Figure 1. Schematic representation of a seeing monitor. The exclamation marks and text in italics show approximations or uncertainties present in any seeing measurements.

a monitor and a telescope can be only made in a statistical sense, with associated non-stationarity errors. Fortunately, in a MASS-DIMM instrument both channels sample the same turbulent path, hence non-stationarity does not affect the precision of the GL seeing estimate.

The seeing is not a well-defined physical quantity like length or mass, so the intrinsic accuracy of seeing monitors cannot be arbitrarily high. It is unrealistic to expect a relative accuracy better than 1% because the "seeing" cannot be defined with such a high accuracy. It is shown below that keeping biases within few percent is not easy.

2.2   Seeing monitors

A seeing monitor measures some statistical properties of phase and/or amplitude of a light wave at the ground and interprets them in terms of the model parameter, seeing. Several approximations are involved in this process, as illustrated in Fig. 1 and discussed below.

Both DIMM and MASS are sensitive to phase distortions with spatial scales below 1 m where the Kolmogorov model works well. A DIMM with small apertures is not affected by the finite turbulence outer scale L_0 (less than 1% bias on variance for $L_0 > 4$ m, cf. Borgnino, Martin, & Ziad 1992). On the other hand, the absolute image motion in a small 10-cm telescope is influenced by a finite L_0, typically at $\sim$10% level. Thus, a site-testing instrument based on the absolute (non-differential) image motion gives a biased r_0 estimate if L_0 is not known. In practise, such seeing monitors are no longer used because they are also affected by mechanical errors (wind shake, tracking). For the same reasons, the theoretically perfect interferometric method of seeing measurements (Dainty & Scaddan 1975) has not become widely adopted.
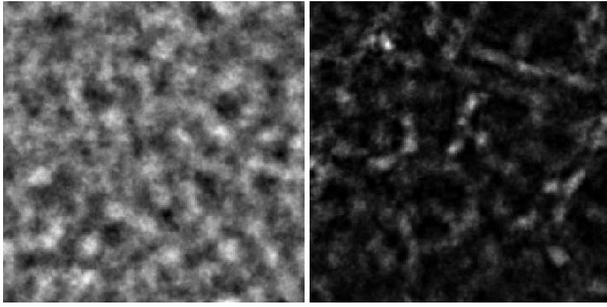
Figure 2. Intensity screens of 1 m^2 size produced by a single turbulent layer and 10 km propagation in conditions of weak scintillation (left, 0.″2 seeing) and strong scintillation (right, 1″ seeing). Wavelength 0.45 μm.

2.3 Propagation

Seeing measurements are affected by the light propagation transforming pure phase distortions to a mixture of phase and amplitude distributions. The spatial spectra of the light phase φ and logarithm of amplitude χ after passing through a weak turbulent layer and propagation over a distance z are

$$\Phi_\varphi(\boldsymbol{f}) = 0.0229\, r_0^{-5/3} |\boldsymbol{f}|^{-11/3} \cos^2(\pi\lambda z |\boldsymbol{f}|^2), \qquad (1)$$

$$\Phi_\chi(\boldsymbol{f}) = 0.0229\, r_0^{-5/3} |\boldsymbol{f}|^{-11/3} \sin^2(\pi\lambda z |\boldsymbol{f}|^2). \qquad (2)$$

The spectrum of intensity fluctuations (scintillation) is $\Phi_I = 4\Phi_\chi$. The amplitude and phase are not correlated at any given point, but their cross-spectrum is not zero at $\boldsymbol{f} \neq 0$, being proportional to the product of the sine and cosine terms.

The *scintillation index* s^2 is defined as

$$s^2 = \langle \Delta I^2 \rangle / \langle I \rangle^2, \qquad (3)$$

where I is the instantaneous light intensity received through some aperture, ΔI is its fluctuation. In the small-perturbation regime, $s^2 \ll 1$, formula (3) is equivalent to the variance of the $\log I = 2\chi$. The scintillation index is calculated then by integrating the amplitude spectrum (2) with a suitable aperture filter. The effect of several turbulent layers is simply additive.

The equations (1) and (2) are only approximate for a real (not weak) turbulence. Even near the zenith, scintillation indices $s^2 > 1$ were measured. This regime of strong scintillation corresponds to the onset of focusing when the deviations from the standard theory become quite significant. Figures 2 and 3 show simulated scintillation signals and their spatial power spectra for weak and strong scintillation (cf. Sect. 2.4). In the latter case, the pattern is dominated by small spikes due to focusing of the light by the "lenses" created by the high-atmosphere turbulence. The size of these spikes is less than the size of the lenses and, accordingly, the power at high spatial frequencies increases compared to the weak-scintillation spectrum (2), while at low frequencies it decreases. The appearance of extra power can be explained qualitatively in the following way. Under weak scintillation, each sinusoidal component of the phase screen creates intensity modulation with the same frequency. As the amplitude of the phase perturbation increases, the phase gratings start to produce second and higher-order or crossed harmonics in the inten-
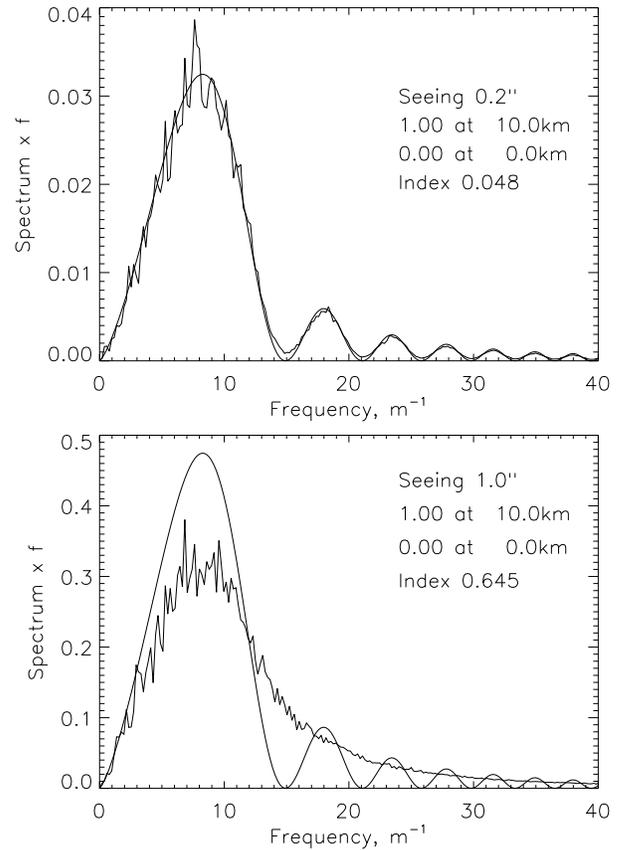

Figure 3. Radially-averaged power spectra of scintillation corresponding to the two cases of Fig. 2. 'Noisy' curves – simulated, smooth curves – weak-perturbation theory, Eq. 2.

sity distribution at the ground. Individual layers are no longer independent but cross-modulate each other. The phase is affected by the saturation in a similar way as the amplitude.

2.4 Simulation tool

Given the lack of accurate wave-propagation theory, the best way to study higher-order propagation effects is by numerical simulation. Simulations are also indispensable in evaluating various instrumental effects.

We use the Fourier method of generating random phase screens with Kolmogorov statistics. A 2-dimensional array of zero-mean Gaussian complex random numbers is created, their amplitudes $\propto \sqrt{C} |\boldsymbol{f}|^{-11/6}$ ($\boldsymbol{f}$ is the spatial frequency, C is the coefficient from Table 1) and phases distributed uniformly in the interval $(-\pi, \pi)$. The Fourier transform (FT) of this array creates the phase screen. It is well known that this method underestimates the low-frequency components of turbulence, and, notably, produces wrong phase structure functions. The reason is that any function obtained by discrete FT is periodic, with a period equal to the grid size. However, the effects of the numerical outer scale can be neglected if the aperture size is a small

fraction of the screen size. Indeed, we checked that in the weak-perturbation regime our numerical simulations reproduce the analytical scintillation spectra and DIMM response to within 2%.

The propagation of wave-fronts is calculated by the spectral technique. If $U_1(\boldsymbol{r})$ is the amplitude of the light wave before propagation, and $\tilde{U}_1(\boldsymbol{f})$ is its FT, then the FT of the amplitude $\tilde{U}_2(\boldsymbol{f})$ after propagation over a distance z is obtained by frequency filtering:

$$\tilde{U}_2(\boldsymbol{f}) = \tilde{U}_1(\boldsymbol{f}) \exp(-i\pi z\lambda|\boldsymbol{f}|^2). \qquad (4)$$

This method is computationally fast, involving only two FTs. Its drawback is that in fact it describes the propagation in a waveguide with a cross-section equal to the simulation grid and reflective walls. However, the propagation of periodic phase screens does not present problems near the grid boundaries because the amplitude "wraps around" the simulated domain boundaries and does not produce artifacts.

We generate large screens of complex light amplitudes at the ground resulting from the propagation through one or several turbulent layers at various altitudes. Typically, with 1024^2 points and 0.5 cm sampling the grid size is 5.12 m. To simulate the data sequence of a seeing monitor, the screens are shifted in both coordinates by $V\tau$, where V is the wind speed and τ is the sampling time interval. The shift is directed at some small angle with respect to the x-axis. In this way, the aperture moves mostly in x but is displaced in y by ~ 0.2 m per line, eventually covering the whole screen one or several times. There are no adverse effects at the borders because the screens are periodic. The statistical averaging is sufficient to simulate typical 1-min measurements.

The complex amplitude of light at the aperture of a seeing monitor is re-sampled on a finer grid and used to calculate the measured quantities such as the spot images in DIMM or fluxes in MASS. The effects of finite CCD pixels and detector noise can be studied as well. The current simulator has some limitations. The wind speed is common to all layers. The blur during a finite exposure time in DIMM is not simulated. In MASS, we simulate the exposure time τ by a linear blur of the apertures over a distance $V\tau$. The simulation is usually monochromatic.

3 ACCURACY OF THE MASS METHOD

3.1 From scintillation to seeing

The MASS instrument is based on the spatial analysis of intensity fluctuations at the ground level. The spatial scale of the scintillation "speckle" produced by turbulence at a distance z is of the order of the Fresnel radius $r_F = \sqrt{\lambda z}$, i.e. ~ 10 cm for a 10-km propagation (Roddier 1981). The spectrum (2) reaches maximum at the spatial frequency $|\boldsymbol{f}| \sim r_F^{-1}$.

Light from a bright star is detected in MASS with four concentric annular apertures with diameters from 2 cm (inner) to 8 cm (outer). The size of these apertures is of the order of r_F and they act jointly as a spatial filter, permitting to dis-entangle scintillation originating at different altitudes. This is achieved in several steps.

Step 1. The sequences of photon counts from 4 apertures with individual micro-exposure of 1 ms are acquired and processed to calculate 10 *scintillation indices* – normal indices s_A^2 for each aperture A and 6 differential indices s_{AB}^2 for pairs of apertures A and B. The formulae for calculating the indices and subtracting the bias caused by the photon noise are given in (Tokovinin et al. 2003). The indices s_A^2 and s_{AB}^2 are equal to the variance of the natural logarithms $\log I_A$ and $\log(I_A/I_B)$ in the limit of small fluctuations of the light intensities I_A and I_B, $s^2 \ll 1$. The turbulence theory usually operates with the variance of the logarithm. However, we measure the photon counts which can be zero and fluctuate even at constant light, hence the indices should be calculated from the normal (non-logarithmic) variances.

Step 2. A linear relation between the observables (indices) and the turbulence profile $C_n^2(z)$ is established by the weak-perturbation theory,

$$s_k^2 = \int W_k(z) \, C_n^2(z)\mathrm{d}z, \qquad (5)$$

where the *weighting function* (WF) $W_k(z)$ describes the altitude response of a given aperture or aperture combination k. For a weak Kolmogorov turbulence, the WF depends *only* on the aperture geometry and spectrum of detected radiation and can be derived from (2) (Tokovinin 2002b, 2003). A normal index for an aperture of diameter D_A corresponds to the low-pass filtering of scintillation, passing $|\boldsymbol{f}| < 1/D_A$, whereas a differential index corresponds to a band-pass spatial filter with $1/D_B < |\boldsymbol{f}| < 1/D_A$. Thus, MASS with its centimetric apertures is sensitive to the turbulence of centimetric scales where the Kolmogorov model is adequate.

It has been shown that the differential index in two concentric annular apertures is almost independent of the propagation distance z for $z > z_{AB} = D_{AB}^2/\lambda$, where $D_{AB} = (D_A + D_B)/2$ is the average aperture diameter (Tokovinin 2002b, 2003). It means that the scintillation index gives a direct measure of the turbulence integral, hence seeing, produced at distances beyond z_{AB}. On the other hand, normal scintillation indices increase as z^β, with $\beta = 5/6$ for small distance $z \ll D^2/\lambda$ and $\beta = 2$ for $z \gg D^2/\lambda$ (Roddier 1981). Accordingly, most of the scintillation is produced by the high layers.

Step 3. Using the known WFs, the set of 10 indices is fitted with a model of 6 thin turbulent layers at altitudes h_i of 0.5, 1, 2, 4, 8, and 16 km, with turbulence integrals J_i in each layer as parameters (Tokovinin et al. 2003). The zenith angle γ is taken into account by the model, $z = h \sec\gamma$. In reality, the turbulence is distributed continuously in altitude with a profile $C_n^2(h)$. The integrals J_i delivered by MASS are approximately equal to $\int C_n^2(h)R_i(h)\mathrm{d}h$, where the *response functions* $R_i(h)$ resemble triangles in $\log h$ coordinate centred on h_i (Tokovinin et al. 2003). The sum of all $R_i(h)$ is close to one for $h > 0.5$ km.

3.2 Over-shoots and their correction

MASS relies on the small-perturbation theory, assuming that the scintillation is weak, $s^2 \ll 1$, and that the combined effect of
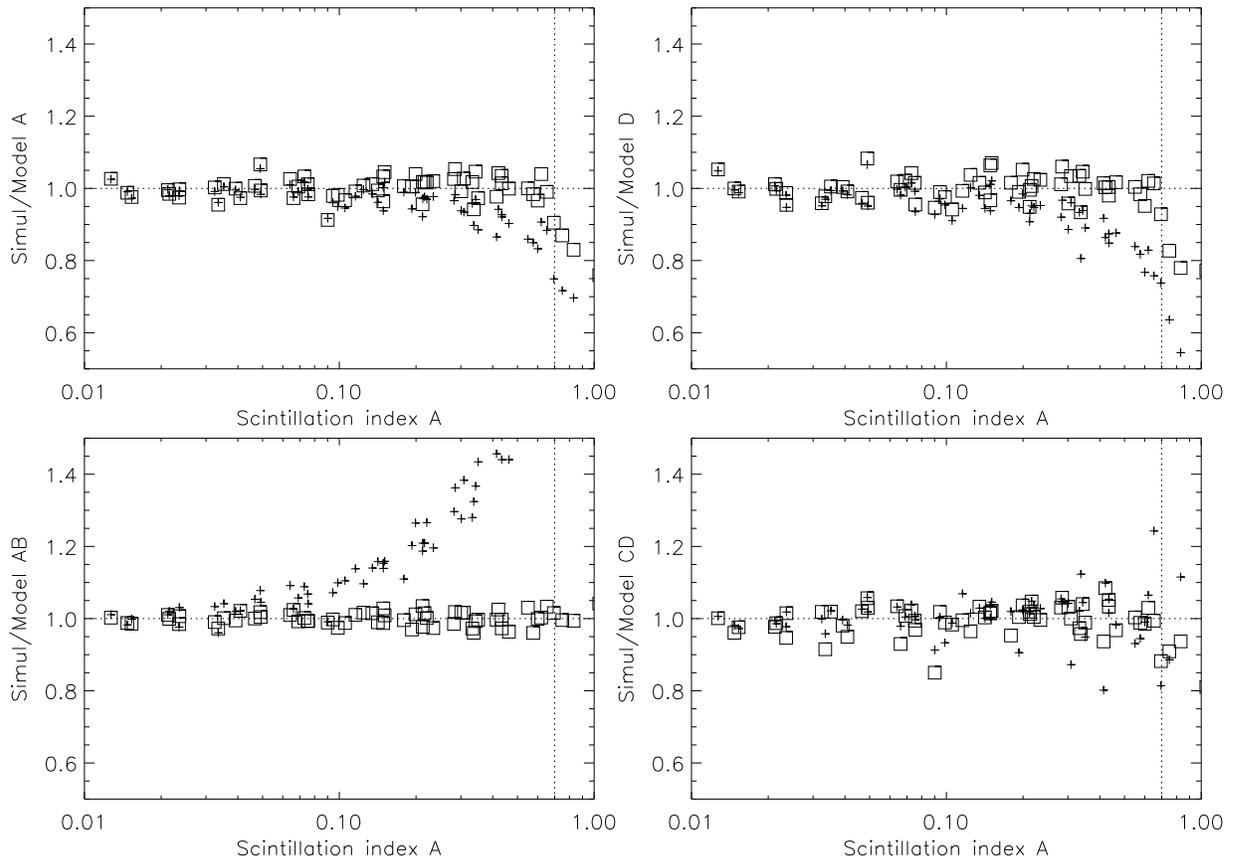
Figure 4. Ratio of measured to modelled scintillation indices. Selected normal (top row) and differential (bottom row) indices in some MASS apertures as determined from the simulations without correction (s^2, crosses) or after correcting by Eq. 6 (s^2_*, empty squares) are divided by the weak-scintillation indices s^2_0. The dotted vertical line marks the correction limit $s^2_A = 0.7$.

several turbulent layers is additive (Eq. 5). In practise, scintillation is not always weak (Sect. 2.3). In this case, profile restoration by the linear method, as implemented in MASS, leads to the over-estimated total turbulence integral (free-atmosphere seeing) and to the shift of the restored profile to lower altitudes.

Although the theory of strong scintillation has been addressed in many papers (e.g. Andrews et al. 1999, and references therein), there is no quantitative description of the intensity power spectrum available. In order to extend MASS operation to moderately strong scintillation, we rely exclusively on numerical simulations (Sect. 2.4). Poly-chromatic light was simulated by an equal mix of three wavelengths of 0.4, 0.45, and 0.55 μm. One or two phase screens at various altitudes were simulated. The physical size of simulated phase screens is 2.5 m across, with 2.5 mm pixels. The power spectrum of intensity fluctuations at the ground was computed (e.g. Fig. 3) and converted into normal and differential scintillation indices of MASS by integrating it with suitable spatial filters.

The values of the measured indices inform us on the strength of the scintillation. Our approach is to correct the measured indices semi-empirically and to bring them into agreement with the weak-scintillation theory. Let s^2 be the 10-element vec-

tor of measured indices, s^2_0 – the vector of theoretical indices expected in the linear theory without saturation, and s^2_* – the vector of corrected indices. A rather general correction formula can be written as

$$s^2_* = \frac{s^2}{1 + Zs^2} \approx s^2_0. \qquad (6)$$

The rationale for selecting this formula is that it automatically removes correction for weak scintillation, and that this type of formula works well for the differential indices. Here, Z is the 10×10 *correction matrix*.

We determine the correction matrix Z empirically from the results of simulations, by least-squares fitting. The fitting is restricted to the relevant scintillation range $0.1 < s^2_A < 0.7$ because weak scintillation does not need correction (but adds statistical noise), while correcting stronger scintillation is hopeless. The matrix Z is found by least squares as

$$Z = (SS^T)^{-1}(S^T Y), \quad Y = S/S_0 - 1, \qquad (7)$$

where the matrices S, S_0, Y have dimensions $10 \times M$, M being the number of simulated cases. We simulated both single and double layers at various altitudes with various strengths of each

layer. All results were mixed together in calculating the matrix Z, with a total of $M = 35$ cases satisfying the condition $0.1 < s_A^2 < 0.7$.

Figure 4 demonstrates the success of this approach with plots of the simulated (pluses) and corrected (squares) indices divided by the weak-scintillation ones. The average ratio s_*^2/s_0^2 of all indices differs from 1 by less than 1% after correction, the scatter is also signifi cantly reduced. The best correction is achieved for s_{AB}^2, rms s_*^2/s_0^2 scatter 1.6%, and the worst correction – for s_D^2, rms scatter 4.6%.

The correction of indices with the matrix Z "learned" from the simulations is implemented in the current version of the MASS software, TURBINA. Old data can be re-processed with this program. An example of successive "overshoot" correction is shown in Fig. 5. Our empirical correction technique works for $s_A^2 < 0.7$. The correction matrix is determined only for the typical aperture diameters and bandpass used in MASS, it has to be revised if these parameters change.

A simplifi ed method of correcting MASS seeing for overshoots has been established earlier and works quite well. If $r_{0,MASS}$ is the Fried parameter of the free-atmosphere seeing measured with the old MASS software, then the corrected r_0 will be

$$r_0 \approx r_{0,MASS} \, (1 + 0.7 s_A)^{0.6}. \tag{8}$$

3.3   Temporal sampling

The photon counts in MASS are sampled with the exposure time $\Delta t = 1$ ms. Averaging the signals during Δt reduces the fluctuations, causing a bias in the measured indices. This bias is corrected in the software by calculating the indices with exposure time Δt and $2\Delta t$ and extrapolating linearly to zero exposure. This extrapolation is calculated as $s_0^2 = 1.5 s_1^2 - 0.5 \rho_1$, where s_1^2 is the measured index and ρ_1 is the covariance with a time lag of 1 sampling period (Tokovinin et al. 2003).

In October 2004 we recorded MASS signals with a faster sampling $\Delta t = 0.25$ ms under rapid-turbulence conditions. It turned out that the linear extrapolation actually over-corrects the indices s_A^2 and s_{AB}^2 by as much as $\sim 6\%$. An analytical study made earlier (Tokovinin 2002b) also concluded that a less drastic correction works better. Accordingly, in the new MASS software the correction is halved, $s_0^2 = 1.25 s_1^2 - 0.25 \rho_1$. The remaining bias is under 2% even on the fastest indices s_A^2 and s_{AB}^2.

3.4   Inner turbulence scale

Turbulence spectrum at high spatial frequencies (comparable to the turbulence inner scale) may have excess power compared to the Kolmogorov model, the so-called *Hill bump* (Andrews et al. 1999). The inner scale is usually of the order of few millimetres, but it can reach centimetric values in the upper atmosphere. This phenomenon can potentially increase the scintillation and lead to over-shoots.

Apart from the extra scintillation, small distortions unaccounted for by the Kolmogorov model must cause excessive image blur, appearing as an extra halo of the PSF. We tried to
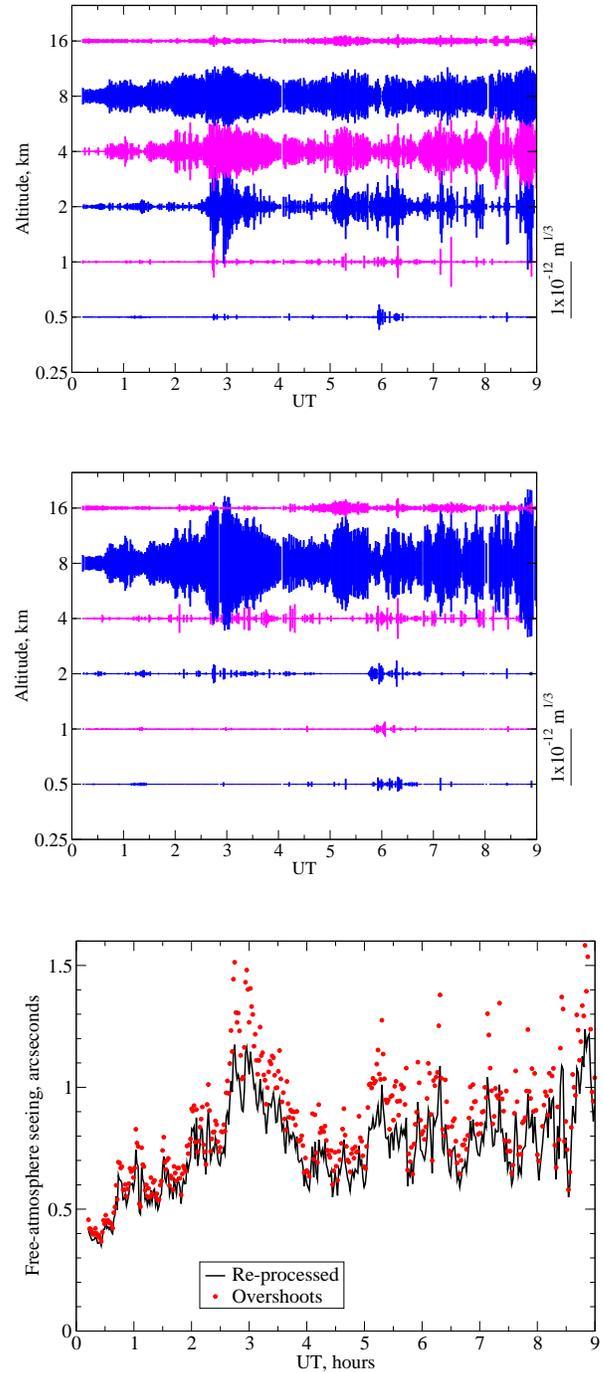

Figure 5. Example of MASS data re-processing. Turbulence profiles at Cerro Tololo for the night of September 30, 2004 are plotted as bars with length proportional to the integrals J_i (cf. the scale on the right). Top – original results, middle – with over-shoot correction. The free-atmosphere seeing calculated from these profiles is compared on the lower plot.
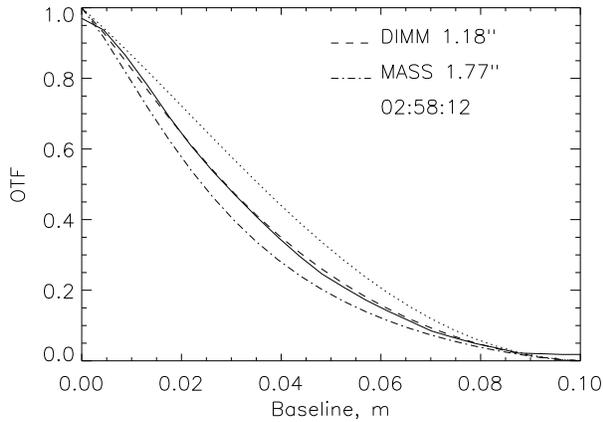
Figure 6. Comparison of the optical transfer function of DIMM spots (full line) with the models based on the Kolmogorov spectrum and the seeing measured by the DIMM (dashed line) and MASS (dash-dotted line) channels. Cerro Tololo, October 1, 2004 2:58UT. The dotted line is a diffraction-limited OTF.

detect such effect by analysing average re-centred images of a star in the DIMM channel of a MASS-DIMM. With 10-cm DIMM apertures, the spots are always diffraction-limited under good seeing, but become broadened as the seeing degrades. Figure 6 shows an example of the 1-dimensional optical transfer function (OTF) of average re-centred DIMM spots in spatial co-ordinate $r = \lambda f$. It is compared to the product of the short-exposure atmospheric and diffraction-limited TFs calculated for $\lambda = 0.55\,\mu\text{m}$ with r_0 measured by both MASS and DIMM. We do not notice any departure from the DIMM model at centimetric scales and conclude that the $1.18''$ seeing adequately described the spot profile, without any perceptible effects of the "Hill bump". On the other hand, MASS over-estimated the seeing because of the un-corrected over-shoots. This analysis was repeated several times on other nights. We conclude that the effect of the finite inner scale on MASS can be safely neglected.

4 ACCURACY OF THE DIMM METHOD

DIMM has a reputation of a "fool-proof" technique for measuring seeing. However, this is not true because its results are affected by optical propagation, centroid algorithm, aberrations, exposure time, noise, etc. Some of these effects can cause a bias much larger than 10%. The accuracy of the DIMM method is studied below by both numerical simulations and analytical theory. The analytics is useful for understanding the small-signal response of a DIMM which turns out to be rather different from the usual assumption that DIMM measures tilts. On the other hand, simulations reveal the faults of the weak-perturbation theory, as for the MASS.

We consider here a DIMM instrument with typical parameters: aperture diameter $D = 10\,\text{cm}$ and baseline $B = 25\,\text{cm}$. In the numerical simulations, we selected a pixel scale of $0.''32$ and a field size of $10'$ around each spot. The complex amplitude of the monochromatic ($\lambda = 0.5\,\mu\text{m}$) light waves at the ground after

propagation through turbulence was calculated with 1 cm sampling (Sect. 2.4). The same amplitude screens can be re-used with varying DIMM parameters (e.g. aberrations). The simulated baseline is 0.24 m (even number of pixels). The centroid window follows the spot, as in typical DIMM instruments, because otherwise the spots would move with respect to the window and the response under bad seeing would be diminished. With 4000 spot pairs in a typical simulation, the statistical error of the differential variance (hence of the derived response coefficients) is 1.6%. Apart from the statistical errors, subtle details of the algorithm and its implementation may influence the results of simulations, which are not *exact* in the absolute sense.

4.1 Response coefficient of an ideal DIMM

In a DIMM, two circular portions of the wavefront are isolated. The variance of the differential wave-front tilts in longitudinal (parallel to the base) σ_l^2 and transverse σ_t^2 directions is related to the Fried parameter r_0 as (Martin 1987; Sarazin & Roddier 1990; Tokovinin 2002a)

$$\sigma_{l,t}^2 = K_{l,t}\,(\lambda/D)^2\,(D/r_0)^{5/3}. \tag{9}$$

The *response coefficients* of DIMM K_l and K_t depend on the B/D ratio and on the kind of the tilt measured. Usually, the tilt is evaluated from the centroids of two stellar images formed by the sub-apertures; in this case it corresponds to the wave-front gradient (G-tilt). The response coefficients for the G-tilt as a function of $b = B/D$ can be approximated by the formulae (Tokovinin 2002a)

$$\begin{aligned} K_l &= 0.340\,(1 - 0.570b^{-1/3} - 0.040b^{-7/3}) \\ K_t &= 0.340\,(1 - 0.855b^{-1/3} + 0.030b^{-7/3}). \end{aligned} \tag{10}$$

For our example, $b = 2.5$, $K_l = 0.1956$, and $K_t = 0.1270$.

The r_0 parameter (and seeing) is computed from the measured differential image-motion variance σ_l^2 by inverting Eq. 9. Hence, it is proportional to the response coefficients to the power 3/5. A 10% error in the response entails a 6% error in seeing.

4.2 Response of the centroid algorithm

In a real DIMM instrument, the image motion is estimated by calculating centroids of the spots. Only a sub-set of detector pixels is used in order to reduce the influence of the noise. These pixels are selected either by setting a threshold well above the background noise or by defining a window around the brightest pixel. Both approaches can be expressed by a general formula

$$c_x = \sum_{i,j} w_{i,j} x_{i,j} I_{i,j}/I_0, \quad I_0 = \sum_{i,j} w_{i,j} I_{i,j}, \tag{11}$$

where c_x is the estimated centroid x-coordinate, $I_{i,j}$ are pixel intensities, $x_{i,j}$ are their x-coordinates. The weights $w_{i,j}$ equal one for selected pixels and zero otherwise, although a more sophisticated weighting scheme could be adopted. Here we explore circular windows where $w = 1$ for pixels at a distance less than $\delta\lambda/D$ from the spot centre. The parameter δ defines the radius of the centroid window in units of the diffraction spot size λ/D.
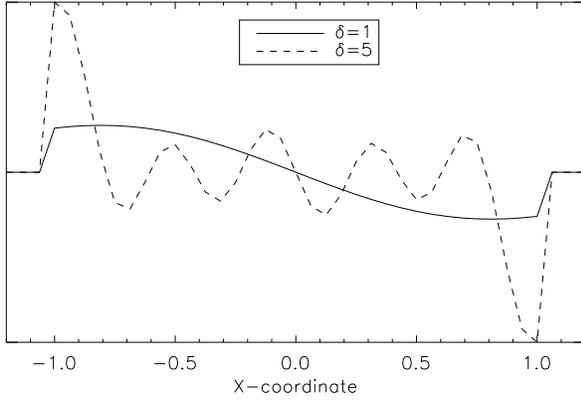
Figure 7. Cuts through the centroid filter functions $F_\varphi(\boldsymbol{x})$ in the x-direction are plotted in arbitrary units against normalised x-coordinate, where ± 1 corresponds to the pupil border. Two centroid windows: narrow $\delta = 1$ and wide $\delta = 5$. No aberrations, $D = 0.1$ m.

Formula (11) is only an approximation to the true image centroid. As a result, the response coefficient of a DIMM is not exactly equal to its theoretical value for G-tilt, but rather depends on the details of centroid calculation. We developed an analytical formula relating the distribution of the light phase and amplitude at the pupil to the change of the image centroid Δc_x (Appendix A), valid for small perturbations. It is analogous to the Taylor expansion of PSF developed for high-contrast imaging (Perrin et al. 2003). The centroid shift Δc_x is equal to the sum of the integrals of atmospheric perturbations $\varphi(\boldsymbol{x})$ and $\chi(\boldsymbol{x})$ multiplied by the *filter functions $F_\varphi(\boldsymbol{x})$ and $F_\chi(\boldsymbol{x})$*, respectively. Knowing the spectra of the perturbations, we calculate the small-signal response coefficients of a DIMM with Eq. A9. The relative accuracy of our calculation is 3% or less.

Figure 7 shows the filter functions of the centroid estimator (11) in the pupil plane calculated by Eqs. A7,A8. For a narrow ($\delta = 1$) centroid window, the filter resembles remotely a Zernike tilt, while for a wide ($\delta = 5$) window it is closer to a gradient averaged over the aperture (opposite spikes at the edges). The DIMM optics is assumed perfect, therefore the centroid is insensitive to amplitude fluctuations at the pupil (scintillation), $F_\chi(\boldsymbol{x}) = 0$.

The situation becomes more complicated when we consider a realistic DIMM instrument with some optical aberrations. In this case, the centroid c_x is affected by both phase and amplitude fluctuations at the pupil (Fig. 8). This effect can be understood qualitatively: a defocused spot resembles a pupil image, hence the centroid estimator becomes sensitive to the gradient of pupil illumination. Sequences of simulated spot images (Fig. 9) illustrate this situation. In a DIMM with perfect optics, the spots are sharp, while their intensities fluctuate because of the scintillation. The defocused spots look more distorted by the same seeing and their centroids move more, biasing the measurements.

The aberrations are characterised here by the amplitude of the Zernike polynomials representing the phase *on each DIMM sub-aperture*. They should not be confused with the aberrations
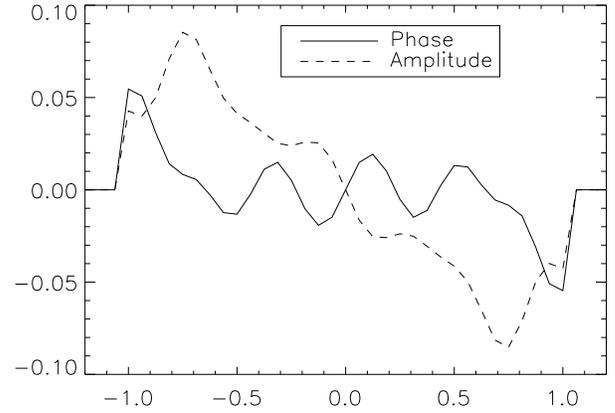

Figure 8. Centroid filter functions $F_\varphi(\boldsymbol{x})$ and $F_\chi(\boldsymbol{x})$ for a defocus of 1 radian rms and $\delta = 5$. Compare with Fig. 7.
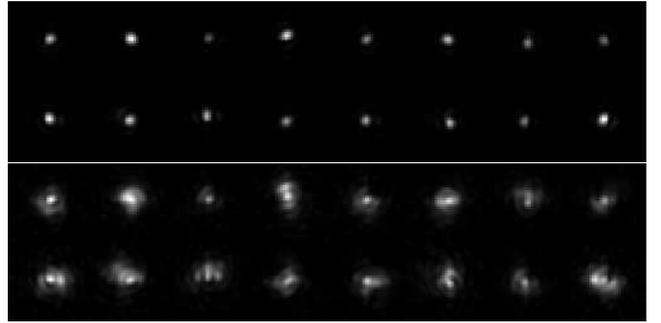

Figure 9. Sequences of simulated spot pairs produced by a turbulent layer at 10 km with $r_0 = 0.1$ m in a DIMM with perfect optics (top) and with a defocus of 1 rad (bottom). The same phase screen is used in both cases.

of the feeding telescope. For example, a coma or spherical aberration in the telescope causes mostly astigmatism in the DIMM sub-apertures. Generally, the aberrations of both sub-apertures are not equal, but, to simplify, we assume here their equality.

4.3 Propagation effects in DIMM

The standard DIMM theory (Martin 1987; Sarazin & Roddier 1990) considers only near-field turbulence and neglects the propagation effects. DIMM is affected by three different phenomena related to propagation.

Diffraction: part of the small-scale phase distortions are converted into amplitude fluctuations (scintillation) according to Eq. 1 and, as a result, the small-signal response of a DIMM slightly decreases with the propagation distance z. The decrease becomes noticeable for $\sqrt{\lambda z} \gtrsim D$ (Tokovinin 2002a), as can be seen in Figs. 10–12 and 14.

Saturation. The second, even stronger effect is caused by the departure from the weak-perturbation theory and becomes important as soon as the scintillation index s_D^2 exceeds 0.1. Simulations show that the response of a perfect DIMM to high-
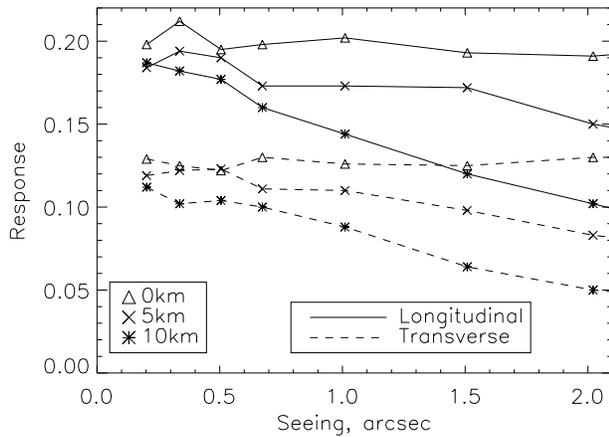
Figure 10. Effect of propagation in a DIMM with $D = 0.1\,\mathrm{m}$, $B = 0.24\,\mathrm{m}$, and perfect optics. Monte-Carlo simulations with $\lambda = 0.5\,\mu\mathrm{m}$ and a single turbulent layer with different seeing located at the ground, at $5\,\mathrm{km}$, and at $10\,\mathrm{km}$.
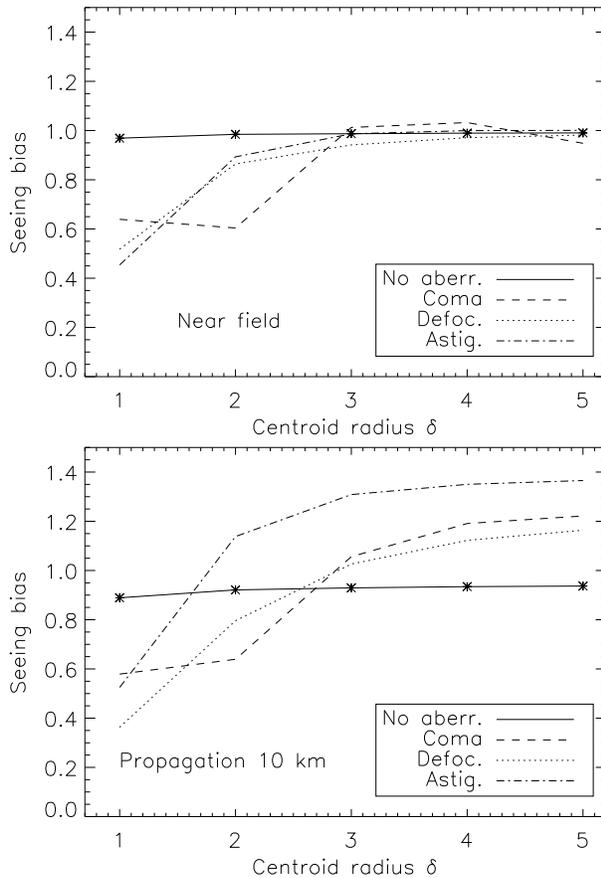

Figure 11. Bias in the seeing estimated from the average longitudinal and transverse image motion (Eq. 12) as a function of the centroid window radius δ for near field (top) and 10 km propagation (bottom). The r.m.s. amplitude of the aberrations (coma a_8, defocus a_4 and astigmatism a_5) is 1 radian. Parameters: $D = 0.1\,\mathrm{m}$, $B = 0.25\,\mathrm{m}$.

altitude turbulence is non-linear, i.e. the coefficients K_l and K_t depend on the seeing (Fig. 10). At $0.''2$ seeing, in the small-signal regime, the response is reduced only by diffraction. The saturation causes additional loss of response, depending on the seeing and layer altitude. On the other hand, the response to the near-ground turbulence remains constant even for a $3''$ seeing, despite strong distortions of the spots which split into several speckles. In practise, situations with $s_{\mathrm{D}}^2 > 0.2$ are not uncommon and a DIMM is expected to "under-shoot". We could model this effect in the same way as we did for the MASS. In order to correct for the under-shoots, we need to know the turbulence profile.

Aberrations together with propagation cause a complex bias considered in the next Section. It would be premature to correct DIMM for saturation and diffraction before the aberration bias is addressed.

4.4 Aberrated DIMM and propagation

Small-signal response coefficients of an ideal and aberrated DIMMs are calculated with (A9) and translated into the bias in the seeing $\varepsilon/\varepsilon_0$ derived from average longitudinal and transverse image motion,

$$\varepsilon/\varepsilon_0 = [(K_l/K_{l,0})^{3/5} + (K_t/K_{t,0})^{3/5}]/2, \qquad (12)$$

where the coefficients $K_{l,0}$ and $K_{t,0}$ of an ideal DIMM are calculated by Eq. 10. This bias is plotted in Fig. 11 as a function of the centroid window radius δ for two cases, turbulence at the ground (near field) and at 10 km distance. Both DIMM apertures have the same aberration. In the near-field case, the response is relatively stable against aberrations, as long as the centroid window is wide enough, $\delta > 2.5$.

When the spots are aberrated, the variance of the differential image motion produced by a high turbulent layer depends on the type of the aberration, its amplitude, propagation distance, and the radius of the centroid window δ (Fig. 11).

The dependence of the DIMM bias on the defocus amplitude is further explored in Fig. 12. Even for zero defocus, there is a small difference in the response between $z = 0$ and $z = 10\,\mathrm{km}$ because of the diffraction. The difference becomes larger for defocused spots. The influence of a small defocus depends on its sign: on one side of the focus, the response decreases and DIMM "under-shoots", on the other side it increases. A defocus larger than 0.8 rad always causes a positive bias. These analytical calculations are confirmed by simulations. When $r_0 = 0.5\,\mathrm{m}$, the simulated response closely follows the small-signal curves. For $r_0 = 0.1\,\mathrm{m}$, the near-field response still matches the theory, but the 10-km response is reduced additionally by the saturation (Fig. 10).

A negative bias caused by the combination of propagation and small defocus may appear counter-intuitive: we expect that scintillation adds something to the image motion produced by the phase. Figure 13 illustrates this effect from the geometric-optics perspective. Suppose that longitudinal image motion in a DIMM is created by a sinusoidal wavefront with a period $\approx 2B$. After propagation, the phase is reduced only slightly, but some amplitude fluctuations are created, positive where the rays converge and negative where they diverge (amplitude fluctuations
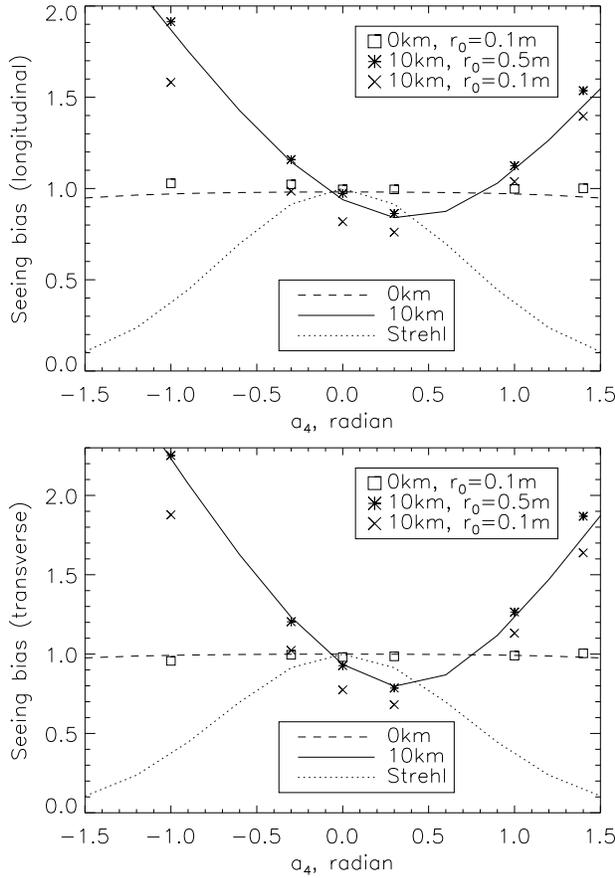
Figure 12. Bias of the seeing derived from the longitudinal (top) and transverse (bottom) image motion in a DIMM with $D = 0.1$ m, $B = 0.25$ m, $\delta = 5$ for turbulent layers at the ground (dashed lines) and at 10 km (full lines), as a function of the Zernike defocus coefficient a_4. The curves show analytical calculations for small signal, the results of simulations for $r_0 = 0.1$ m and $r_0 = 0.5$ m are over-plotted with symbols. The dotted lines indicate Strehl ratio.
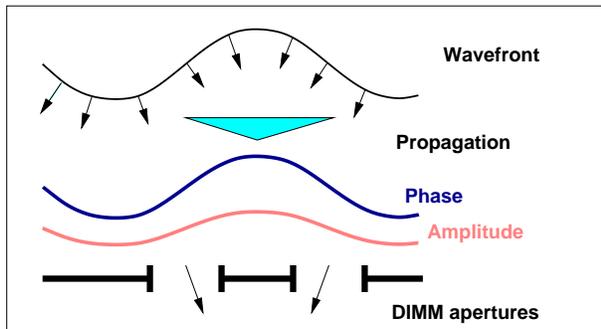

Figure 13. Illustration of the propagation effects in a DIMM (see text).
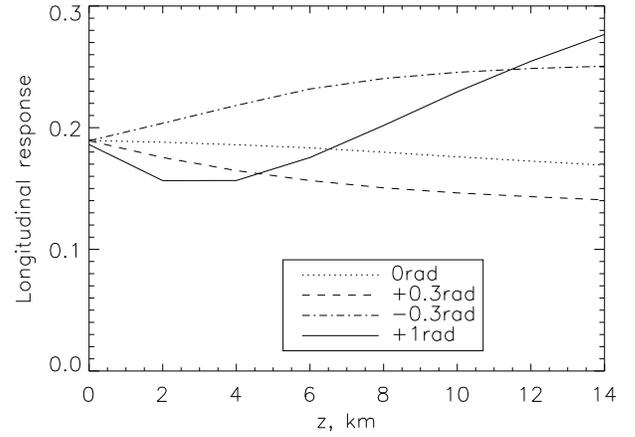

Figure 14. The dependence of longitudinal small-signal response coefficient K_l of a DIMM with $D = 0.1$ m, $B = 0.25$ m, $\delta = 5$ on the propagation distance z for four values of defocus indicated on the plot. The behaviour of the transverse coefficient is similar.

are proportional to the wave-front curvature). The gradient of the amplitude at DIMM apertures is correlated with the phase gradient (i.e. image motion). A perfect DIMM is insensitive to the amplitude fluctuations, but in a defocused DIMM the centroids are affected by the amplitude gradients. Depending on the sign of the defocus, the amplitude gradient either increases or decreases the measured image motion and thus creates a positive or negative bias.

A positive bias caused by strong defocus (and other aberrations) has been confirmed experimentally by direct comparisons between well-aligned and aberrated DIMMs (Wang et al. 2006). The negative bias found here has not been suspected before. A defocus of 0.3 rad rms (24 nm for $\lambda = 0.5\,\mu$m) corresponds to a Strehl ratio of 0.91, i.e. practically diffraction-limited spots. Yet, such a DIMM can have response coefficients reduced or increased by $\sim$20%, and will produce seeing data biased by $\sim \pm$12% when most of the turbulence is concentrated at 10 km. Optical aberrations other than defocus are expected to cause a similarly complex bias. We conclude that *the response of a DIMM to high-altitude turbulence is intrinsically inaccurate*. The saturation makes things even worse, introducing dependence of the response on turbulence profile.

We simulated the centroid calculation by *thresholding* numerically and found that its behaviour is very similar to the windowing method considered above. For turbulence at the ground, the response is insensitive to aberration, but slightly depends on the threshold (a bias of +10% in K_l and K_t for a threshold of 0.1). The asymmetric dependence of response to high-altitude turbulence on the defocus (Fig. 12) is also preserved.

Figure 14 shows how the small-signal response depends on the propagation distance z. For un-aberrated spots, the response slowly decreases with z. On the other hand, defocused spots show both positive and negative bias. A real DIMM instrument can either "over-shoot" or "under-shoot", depending on the state of its optics and the turbulence profile.

It is clear that the quality of the DIMM optics and focus has to be strictly controlled in order to get unbiased results. Measurement of the spot Strehl ratio (SR) suggested in (Tokovinin 2002a) is helpful, with SR> 0.5 usually indicating acceptable quality (Wang et al. 2006). However, the SR is reduced under poor seeing even in a perfect DIMM, so if the data with poor SRs are rejected, the seeing statistics will be biased. Yet another way to quantify the aberrations in a DIMM will be to take long exposures of defocused spots and to analyse them with the method described by Tokovinin & Heathcote (2006). Needless to say that a DIMM working always out-of-focus (e.g. Bally et al. 1996) will never measure the seeing accurately.

4.5 Exposure-time bias

Finite exposure time in a DIMM reduces the differential image motion, biasing the measured seeing to smaller values. The effect can be quite strong, as noted by Martin (1987). This bias was modelled in detail in (Tokovinin 2002a). Short (e.g. 5 ms) exposures reduce the bias, but do not eliminate it completely. If the data is acquired continuously, an extrapolation to zero-exposure can be done from the variances of time-binned signal, either by fitting an exponential curve to the dependence of the variance on exposure time (Wang et al. 2006) or by using a simple linear formula as in MASS or GSM (Ziad et al. 2000). The linear extrapolation appears too strong, though.

If the image sequence is not continuous, a method of interlaced single and double exposures should be used. In this case, a "modified exponential correction" was developed in (Tokovinin 2002a)[1]. If ε_1 and ε_2 are the seeing values calculated with nominal and double exposure time, the de-biased seeing ε_0 is estimated from

$$\varepsilon_0 \approx 0.5(c_1\varepsilon_1 + c_1^{7/3}\varepsilon_2), \tag{13}$$

where $c_1 = (\varepsilon_1/\varepsilon_2)^{3/4}$. To reduce the statistical noise, the factor c_1 is averaged (smoothed) over time and its average value is then used in (13) to correct individual measurements.

4.6 Centroid noise

Even in the absence of atmospheric image motion, the measured centroids fluctuate because of the errors caused by the photon noise and detector readout noise. The errors of intensities $I_{i,j}$ are independent in each pixel and equal to the sum of readout and Poisson noise, expressed in the signal counts (ADU):

$$\sigma_{I_{i,j}}^2 = R^2 + I_{i,j}/G, \tag{14}$$

were R is readout noise in ADU, and G — the CCD camera conversion factor (gain) in e^-/ADU. The influence of these errors on the calculated centroid is easily evaluated by differentiating Eq. 11 and using independence of noise in each pixel. As the

weights $w_{i,j}$ take values of either 1 or 0, we simply restrict the summation to pixels where $w_{i,j} = 1$. The result is

$$
\begin{aligned}
\sigma_c^2 &= \frac{1}{I_0^2}\sum_{i,j}(x_{i,j} - c_x)^2 \sigma_{I_{i,j}}^2 \\
&= \frac{1}{I_0^2}\sum_{i,j}(x_{i,j} - c_x)^2(R^2 + I_{i,j}/G) \tag{15}
\end{aligned}
$$

Here I_0 is the sum of intensities over pixels in the centroid window.

The sum entering in (15) can be computed in advance if the centroid window has a well-defined size and the image profile is known. This is not the case when a thresholding method is used. However, even with thresholding the centroid noise of each individual spot can be evaluated with (15) during centroid computation. Variations of the flux caused by scintillation or clouds can be accounted for as well.

Obviously, the noise variance of both centroids in the DIMM has to be evaluated and subtracted from the measured differential variance before calculating the seeing with (9). It would be wrong to express the noise in arc-seconds and subtract it later from the measured seeing, because the effects in the longitudinal and transverse directions are not the same. The noise depends on the stellar flux, hence subtracting a fixed "instrumental noise" is not correct. Typically, the noise is small and its subtraction or not does not matter. However, the noise can significantly bias DIMM results under good seeing or for faint stars. The flux in the interlaced single and double exposures is different, hence if the noise variance is not properly subtracted, it will bias (over-estimate) the correction (13).

To reduce the noise, especially the term related to R, the smallest number of pixels must be used, favouring a narrow centroid window with $\delta \sim 1$ or, equivalently, a high threshold. However, we have seen in Sect. 4.2 that such choice leads to a very uncertain response coefficient in presence of even small aberrations. The noise is usually much less of a problem than the aberrations, so a wide centroid window with $\delta \geqslant 2.5$ or a low threshold are preferable, contrary to the recommendation given in (Tokovinin 2002a).

Both the measurement noise and the noise caused by the scintillation are isotropic and affect longitudinal and transverse image motion equally. The effect on the calculated seeing, however, will be different because $K_l > K_t$. If the DIMM signal contains a significant noise component, the "transverse" seeing will always be larger than the "longitudinal" seeing. This effect could be mistakenly interpreted as a manifestation of a non-Kolmogorov turbulence spectrum.

5 CONCLUSIONS

This work complements previous studies of two methods to measure seeing – DIMM and MASS – and focuses on the achievable accuracy. The "seeing" itself cannot be defined very accurately, being a model-dependent parameter of a random and non-stationary process. Taking aside this caveat, we investigate potential instrumental biases by simulating both turbulence and

---

[1] Formula 13 in (Tokovinin 2002a) contains a typographic error, corrected here

the instruments numerically. The true seeing is known exactly, permitting to calibrate the methods on the absolute scale.

Our conclusions and recommendations can be summarised as follows:

- The departure from the weak-perturbation theory affects the MASS method seriously, but it is correctable for a not-too-strong scintillation, $s_A^2 < 0.7$.
- The effects of finite exposure time and inner turbulence scale in MASS can be neglected.
- The DIMM method is very robust and tolerant to aberrations for the near-ground turbulence, provided that the centroid calculation uses a large enough radius, $> 2.5\lambda/D$.
- Optical propagation causes a non-linear response of DIMM (saturation), not present in the near-field case.
- Combination of propagation and aberrations in a DIMM leads to a complex bias. By controlling the DIMM optical quality (Strehl ratio > 0.5), we can keep the seeing bias to within $\pm 12\%$, but making the control tighter appears impractical.
- Centroid noise in a DIMM should be computed and subtracted from the measured variance. To do so, the detector readout noise and gain must be known.
- The exposure-time bias in a DIMM should be corrected using one of several known recipes.

The sensitivity of the DIMM to propagation and aberrations comes as a surprise, although neither of these effects was accounted for by the standard, near-field DIMM theory. The bias on high-altitude seeing is so complex that removing it completely seems unrealistic.

It has been demonstrated that two identical DIMM instruments with good optics can give seeing measurements concordant to within few percent (Wang et al. 2006). Are these measurements *accurate* to the same level? Not necessarily. A seeing of $1''$ coming from $10\,\mathrm{km}$ could be measured by both instruments with a bias of 0.83 (Fig. 10), whereas the same seeing originating near the ground will be measured correctly.

The response of a DIMM depends on both instrumental factors and observing conditions. Two different DIMMs can agree on one night (e.g. seeing dominated by low layers) and disagree on another night or at another site. Two identical DIMMs can be biased in a different way at two different sites. Thus, inter-comparison between DIMM (or MASS) instruments cannot guarantee that they are *accurate*. Their mutual agreement is a necessary, but not sufficient condition. Only a careful control of biases can ensure accurate seeing data. However, instrument inter-comparisons are useful for debugging and checks and should be pursued whenever possible.

A combination of MASS and DIMM in one instrument has stimulated this research. These instruments, when properly calibrated, agree very well for a seeing dominated by high layers (Kornilov et al. 2007). This is a triumph of the optical propagation theory enabling us to interpret both scintillation and image motion with a common model and a single parameter, r_0. At the same time, the agreement between two instruments based on different principles and with different biases is a strong argument that both are *accurate*, i.e. measure the seeing on the absolute scale.

REFERENCES

Andrews I.C., Phillips R.L., Hopen C.Y., Al-Hanash M.A., 1999, J. Opt. Soc. Am. A, 16, 1417

Bally J., Theil D., Billawalla Y., Potter D., Loewenstein R. F., Mrozek F., Lloyd J. P., 1996, PASA, 13, 22

Borgnino J., Martin F., Ziad A., 1992, Opt. Comm., 91, 267

Dainty J.C., Scaddan, R.J., 1975, MNRAS, 170, 519

Goodman J.W., 1985, Statistical Optics. Wiley, New York

Kenyon S., Lawrence J.S., Ashley M.C.B., Storey J.W.V., Tokovinin A., Fossat E., 2006, PASP, 118, 924

Kornilov V., Tokovinin A., Voziakova O., Zaitsev A., Shatsky N., Potanin S., Sarazin M., 2003, Proc. SPIE, 4839, 837

Kornilov V., Tokovinin A., Shatsky N., Voziakova O., Potanin S., Safonov B., 2007, MNRAS, submitted

Martin H.M., 1987, PASP, 99, 1360

Perrin M.D., Sivaramakrishnan A., Makidon, R.B., Oppenheimer B.R., Graham J.R., 2003, ApJ, 596, 702

Roddier F. 1981, in Wolf E., ed. Progress in Optics, Vol. 19. North-Holland, Amsterdam, p. 281

Sarazin M., Roddier F., 1990, A& A, 227, 294

Tatarskii V.I., 1961, Wave Propagation in a Turbulent Medium. Dover Press, New York

Tokovinin A., 2002a, PASP, 114, 1156

Tokovinin A., 2002b, Appl. Opt., 41, 957

Tokovinin A., 2003, J. Opt. Soc. Am. A, 20, 686

Tokovinin A., Heathcote S., 2006, PASP, 118, 1165

Tokovinin A., Kornilov V., Shatsky N., Voziakova O., 2003, MNRAS, 2003, 343, 891

Tokovinin A., Vernin J., Ziad A., Chun M., 2005, PASP, 117, 395

Wang L., Schoeck M., Chanan G., Skidmore W., Bustos E., Seguel J., Blum R., 2006, in Stepp L.M., ed., Ground-based and Airborne Telescopes, Proc. SPIE, 6267, 62671S

Ziad A., Conan R., Tokovinin A., Martin F., Borgnino. J., 2000, Appl. Opt., 39, 5415

APPENDIX A: RESPONSE OF A CENTROID ESTIMATOR IN THE PUPIL PLANE

The centroid signal c for each DIMM spot is obtained from the weighted PSF $I(\boldsymbol{a})$ as

$$c = I_0^{-1} \int \mathrm{d}^2\boldsymbol{a}\; I(\boldsymbol{a})\; M(\boldsymbol{a}), \tag{A1}$$

where $\boldsymbol{a}$ is a 2-dimensional vector of angular coordinates, $M(\boldsymbol{a})$ is some function, *mask*, and I_0 is the total intensity (flux). All integrals are in infinite limits and exist because all functions are supposed to have limited support. The PSF is not necessarily an ideal one, but may include some aberrations. Formula (A1) is rather general and applies to many situations, e.g. curvature sensing. For centroid calculation, we need a mask $M(\boldsymbol{a}) = a_x w(\boldsymbol{a})$ to match Eq. 11. We keep (A1) in a general form useful for other applications.

Let $\boldsymbol{x}$ be the coordinate vector in the pupil plane. The complex amplitude of the initial un-perturbed field at the pupil is $U(\boldsymbol{x})$. It includes the pupil function (possibly with aberrations) and is normalised arbitrarily. Suppose that the amplitude U is changed by a small phase aberration $\varphi(\mathbf{x})$ and a small log-amplitude perturbation $\chi(\boldsymbol{x})$ and becomes $U(\boldsymbol{x})\; e^{i\varphi(\boldsymbol{x})+\chi(\boldsymbol{x})}$. What would be the change of the signal Δc caused by this aberration?

We find a small change in the signal by linearising the known expression of the OTF (Goodman 1985)

$$\tilde{I}(\boldsymbol{f}) = I_0^{-1} \int \mathrm{d}^2\boldsymbol{x}\; U(\boldsymbol{x})U^*(\boldsymbol{x}+\lambda\boldsymbol{f}) \tag{A2}$$

with respect to small perturbations $\varphi \ll 1$ and $\chi \ll 1$, so-called *PSF Taylor expansion* (Perrin et al. 2003):

$$\begin{aligned}\Delta\tilde{I}(\boldsymbol{f}) &= I_0^{-1} \int \mathrm{d}^2\boldsymbol{x}\, U(\boldsymbol{x})U^*(\boldsymbol{x}+\lambda\boldsymbol{f}) \\ &\times\ [i\varphi(\boldsymbol{x})+\chi(\boldsymbol{x})-i\varphi(\boldsymbol{x}+\lambda\boldsymbol{f})+\chi(\boldsymbol{x}+\lambda\boldsymbol{f})]\end{aligned} \tag{A3}$$

The signal increment is

$$\Delta c = \int \mathrm{d}^2\boldsymbol{f}\; \Delta\tilde{I}(\boldsymbol{f})\tilde{M}(\boldsymbol{f}). \tag{A4}$$

We put (A3) into (A4) and re-group the terms. The first term in the square brackets containing $i\varphi(\boldsymbol{x})$ leads to

$$\begin{aligned}\Delta c_1 &= i(\lambda^2 I_0)^{-1} \int \mathrm{d}^2\boldsymbol{x} \int \mathrm{d}^2\boldsymbol{x}'\; U(\boldsymbol{x})U^*(\boldsymbol{x}+\boldsymbol{x}') \\ &\times\ \tilde{M}(\boldsymbol{x}'/\lambda)\; \varphi(\boldsymbol{x}),\end{aligned} \tag{A5}$$

where $\boldsymbol{x}' = \lambda\boldsymbol{f}$. The 3-rd term containing $-i\varphi(\boldsymbol{x}+\lambda\boldsymbol{f})$ leads to the complex-conjugate of the expression (A5) with inverse sign. Collecting all 4 terms, we write the result as

$$\Delta c = \int \mathrm{d}^2\boldsymbol{x}\; F_\varphi(\boldsymbol{x})\; \varphi(\boldsymbol{x}) + \int \mathrm{d}^2\boldsymbol{x}\; F_\chi(\boldsymbol{x})\; \chi(\boldsymbol{x}), \tag{A6}$$

where the *filter functions* F are

$$F_\varphi(\boldsymbol{x}) = \mathrm{Im}[A(\boldsymbol{x})], \quad F_\chi(\boldsymbol{x}) = \mathrm{Re}[A(\boldsymbol{x})] \tag{A7}$$

© 2007 RAS, MNRAS **000**, 1–13

and

$$A(\boldsymbol{x}) = 2\; (\lambda^2 I_0)^{-1}\; U(\boldsymbol{x}) \int \mathrm{d}^2\boldsymbol{x}'\; U^*(\boldsymbol{x}+\boldsymbol{x}')\; \tilde{M}(\boldsymbol{x}'/\lambda) \tag{A8}$$

The response is independent of the normalisation of the amplitude U because it is divided by the flux.

This result contains an implicit assumption that the fluctuations of the denominator I_0 can be neglected. This is not always true. The signal has the form $c = A/B$, hence its fluctuations are $\Delta c = \Delta A/B - c(\Delta B/B)$. The fluctuations of the denominator ΔB can be neglected if the average signal $c = 0$ (they will be a second-order term then). This condition is enforced by the choice of $M(\boldsymbol{a}) = a_x w(\boldsymbol{a})$ appropriate for a windowed centroid.

If the mask M is correctly dimensioned to compute the centroid c in pixels and the angular size of the pixel is p, then it follows that the longitudinal response coefficient K_l is

$$\begin{aligned}K_l &= (pD/\lambda)^2\; (r_0/D)^{5/3} \int \mathrm{d}^2\boldsymbol{f} \\ &\times\ |\tilde{F}_\varphi(\boldsymbol{f})|^2\; \Phi_\varphi(\boldsymbol{f})[2\sin(\pi B f_x)]^2,\end{aligned} \tag{A9}$$

where both centroid measurement direction and baseline are parallel to the x axis. To calculate the transverse response K_t, we replace f_x with f_y. To take into account both propagation and sensitivity to scintillation, we make a replacement

$$|\tilde{F}_\varphi(\boldsymbol{f})|^2 \to |\tilde{F}_\varphi(\boldsymbol{f})\cos(\pi\lambda z|\boldsymbol{f}|^2)+\tilde{F}_\chi(\boldsymbol{f})\sin(\pi\lambda z|\boldsymbol{f}|^2)|^2. \tag{A10}$$

This modification automatically accounts for the correlation between phase and amplitude.

This paper has been typeset from a TeX/ LaTeX file prepared by the author.